Available online at www.sciencedirect.com

ScienceDirect

Nuclear Physics B 911 (2016) 447–470

NUCLEAR PHYSICS B

www.elsevier.com/locate/nuclphysb

Interpreting the 750 GeV diphoton excess within topflavor seesaw model

Junjie Cao [a], Liangliang Shang [a], Wei Su [b], Fei Wang [a,c,b,*], Yang Zhang [b]

[a] *Department of Physics, Henan Normal University, Xinxiang 453007, PR China*

[b] *State Key Laboratory of Theoretical Physics, Institute of Theoretical Physics, Chinese Academy of Sciences, Beijing 100080, PR China*

[c] *School of Physics, Zhengzhou University, ZhengZhou 450000, PR China*

Received 4 June 2016; received in revised form 12 August 2016; accepted 17 August 2016

Available online 23 August 2016

Editor: Hong-Jian He

Abstract

We propose that the extension of the Standard Model by typical vector-like $SU(2)_L$ doublet fermions and non-singlet scalar field can account for the observed 750 GeV diphoton excess in experimentally allowed parameter space. Such an idea can be realized in a typical topflavor seesaw model where the new resonance X is identified as a CP-even or CP-odd scalar emerging from a certain bi-doublet Higgs field, and it can couple rather strongly to photons and gluons through mediators such as vector-like fermions, scalars as well as gauge bosons predicted by the model. Numerical analysis indicates that the model can predict the central value of the diphoton excess without contradicting any constraints from 8 TeV LHC. Among all the constraints, the tightest one comes from the $Z\gamma$ channel with $\sigma^{Z\gamma}_{8\,\mathrm{TeV}} \lesssim 3.6$ fb, which requires $\sigma^{\gamma\gamma}_{13\,\mathrm{TeV}} \lesssim 6$ fb in most of the favored parameter space. Theoretical issues such as vacuum stability and Landau pole are also addressed.

* Corresponding author.
E-mail address: feiwang@zzu.edu.cn (F. Wang).

http://dx.doi.org/10.1016/j.nuclphysb.2016.08.018

1. Introduction

Recently in the searches for new physics at the LHC Run-II with $\sqrt{s} = 13$ TeV and 3 fb^{-1} integrated data, both the ATLAS and CMS Collaborations reported a diphoton excess with an invariant mass around 750 GeV [1,2]. Combined with the 8 TeV data, the favored rate of the excess is given by

$$\sigma_{\gamma\gamma}^{750\ \mathrm{GeV}} = (4.4 \pm 1.1)\ \mathrm{fb} \tag{1.1}$$

in the narrow width approximation [3]. Although the local significances are not very high, which are only 3.9σ for ATLAS data and 2.6σ for CMS data, this excess is widely regarded as a hint of new physics beyond the Standard Model (SM).

Such an excess was explained in various models [3–15], and the gluon fusion process $gg \to X \to \gamma\gamma$ was usually considered as the source of the excess, where X denotes an assumed scalar particle with its mass around 750 GeV. According to these studies, the interactions of X with the SM particles other than gluons and photons should be significantly weaker than those of the Higgs boson in the SM, and consequently the rates of the X-mediated processes $pp \to X \to ZZ, W^+W^-, hh, f\bar{f}$ are suppressed so that no significant excess of these channels was observed at the LHC Run-I [13]. Besides, X should interact with new charged and colored particles to induce the effective $X\gamma\gamma$ and Xgg couplings through their loop effects. In order to explain the excess in an elegant way, the new particles should be light, and meanwhile their interactions with X must be moderately strong.

Among the new physics models employed to interpret the excess, the minimal theoretical framework is the extension of the SM by one gauge singlet scalar field and vector-like (colored as well as $SU(2)_L$ singlet) fermions [4]. This framework has been extensively discussed since it provides a very simple but meanwhile feasible explanation of the excess. However, as pointed out in [14], in order to account for the excess the needed Yukawa couplings of the fermions are usually large so that the electroweak vacuum state of the scalar potential becomes unstable at a certain energy scale, which implies that other new physics must intervene. This motivates us to go beyond the minimal framework. To accomplish this task, one may change the transform properties of the vector-fermions and/or the scalar under the SM gauge group. For example, one may choose the fermions to be $SU(2)_L$ doublets instead of singlet, and/or the scalar to be non-singlet of the $SU(2)_L$. Contrary to naive expectations, these choices are still allowed by the LHC constraints on WW and ZZ channels. One may also change the interaction of X with the fermions. To be more specific, for the interaction $\lambda_F X\bar{F}F$ with F denoting a vector-like fermion, its contribution to the $X\gamma\gamma$ coupling is determined by the ratio $\frac{\lambda_F}{M_F}$ under the condition $4M_F^2 \gg (750\ \mathrm{GeV})^2$. If this interaction is also responsible for the fermion masses, one can get $\frac{\lambda_F}{M_F} \equiv \frac{1}{v}$, where v is the vacuum expectation value (VEV) of X, and it also represents the scale of new particle in the theory. So in order to get an appropriate contribution to the excess, the value of v should be as low as possible, which makes the theory readily tested at the LHC. On the other hand, if the fermion acquires its mass in a complicated way, e.g. by typical seesaw mechanism, an effective negative contribution to the fermion mass can be generated. As a result, λ_F and M_F can become uncorrelated and their ratio may be much larger than $1/v$. In this case, a large v can still provide a sizable contribution to diphoton excess, and the resulting effective theory at the TeV scale contains only the scalar X and the fermions, which is quite similar to the minimal model.

In this work, we propose a model that incorporates the essential features of the two types of extensions. We are motivated by top-specific models, such as the top condensation models

[16,17] and the top seesaw model [18,19], and assume that the third generation fermions in the SM undergo a different $SU(2)$ weak interaction from the first two generation fermions [20,21]. At the same time, we introduce new vector-like fermions and split their masses by seesaw mechanism. In this way, the particle X is identified as a CP-even or CP-odd scalar emerging from a bi-doublet Higgs, which triggers the breaking of the two SU(2) gauge symmetry into the SM $SU(2)_L$ symmetry, and its interaction with photons is induced by relevant fermions, scalars as well as gauge bosons predicted by the model. We emphasize that in such an explanation, the resonance X is naturally embedded in a scalar sector which is responsible for both the symmetry breaking and generating the masses of the new particles, and the popular seesaw mechanism for fermion sector is utilized to recover the minimal framework at TeV scale for the diphoton excess. Moreover, the stability of the vacuum in the theory can be improved in comparison with the minimal framework. So our explanation is physical and meanwhile economical in model building. We also emphasize that our model is somewhat similar to the topflavor seesaw model proposed in [22], so we dub it hereafter the topflavor seesaw model.

This paper is organized as follows. In section 2, we introduce the structure of the typical top flavor seesaw model, and list its particle spectrum. In section 3, we choose benchmark scenarios to study the diphoton excess. Subsequently we draw conclusions in section 4. We also present more details of our model in the Appendix.

2. The framework of the topflavor seesaw model

In this section, we recapitulate the structure of the typical topflavor seesaw model. This model is based on the gauge symmetry group $SU(3)_c \times SU(2)_1 \times SU(2)_2 \times U(1)_Y$, where the third generation fermions transform non-trivially under the $SU(2)_2$ group, while the first two generation fermions transform by the $SU(2)_1$ group. The breaking of the gauge group into the electromagnetic group $U(1)_Q$ is a two-stage mechanism: firstly the $SU(2)_1 \times SU(2)_2 \times U(1)_Y$ group breaks down into $SU(2)_L \times U(1)_Y$ group at the TeV scale, and subsequently the $SU(2)_L \times U(1)_Y$ symmetry breaks down into the $U(1)_Q$ at the electorweak scale. These breakdown processes can be accomplished by introducing two Higgs doublets and one bi-doublet Higgs with the following $SU(3)_c \times SU(2)_1 \times SU(2)_2 \times U(1)_Y$ quantum numbers

$$H_1 \sim (\,1,\ 2,\ 1)_{-1/2}\,,\ H_2 \sim (\,1,\ 1,\ 2)_{-1/2}\,,\ \Phi \sim (\,1,\ 2,\ 2)_0. \tag{2.1}$$

In this model, we also introduce following vector-like quarks and leptons to couple with the bi-doublet Higgs Φ

$$\begin{aligned}
&V_L \equiv (\mathcal{T}, \mathcal{B})_L \sim (3,2,1)_{1/6}\,,\quad V_R \equiv (\mathcal{T}, \mathcal{B})_R \sim (3,1,2)_{1/6}\,,\\
&V'_R \equiv (\tilde{\mathcal{T}}, \tilde{\mathcal{B}})_R \sim (3,2,1)_{1/6}\,,\quad V'_L \equiv (\tilde{\mathcal{T}}, \tilde{\mathcal{B}})_L \sim (3,1,2)_{1/6}\,,\\
&\tilde{V}_L \equiv (\mathcal{N}, \mathcal{E})_L \sim (1,2,1)_{-1/2}\,,\quad \tilde{V}_R \equiv (\mathcal{N}, \mathcal{E})_R \sim (1,1,2)_{-1/2}\,,\\
&\tilde{V}'_R \equiv (\tilde{\mathcal{N}}, \tilde{\mathcal{E}})_R \sim (1,2,1)_{-1/2}\,,\quad \tilde{V}'_L \equiv (\tilde{\mathcal{N}}, \tilde{\mathcal{E}})_L \sim (1,1,2)_{-1/2}\,,
\end{aligned} \tag{2.2}$$

and write down their mass terms as follows

$$-\mathcal{L} \supseteq M_H \bar{V}_L V'_R + M_H \bar{V}_R V'_L + \bar{V}_L\,(\lambda_V \Phi)\,V_R + \bar{V}'_L\,(\lambda_V \Phi)\,V'_R + (\mathrm{V}, \mathrm{V}' \to \tilde{\mathrm{V}}, \tilde{\mathrm{V}}') + h.c.,$$

where the dimensionful coefficient M_H may have a dynamical origin or just be imposed by hand, and its sign may be either positive or negative. In this work, we set it to be positive, and this choice does not affect our interpretation of the diphoton excess. With the vector-like extensions, we find that anomaly cancelation holds in our model.

With the above field assignments, the remaining Lagrangian is given by

$$\begin{aligned}
\mathcal{L} &\supseteq \mathcal{L}_{kin} + \mathcal{L}_Q + \mathcal{L}_L - V(\Phi) - V(H_1, H_2)\,, \qquad (2.3)\\
-\mathcal{L}_Q &\supseteq \bar{Q}_{3,L}\left(H_2 y_t t_R + i\tau_2 H_2^* y_b b_R\right) + \bar{V}_L\left(H_1 y_T t_R + i\tau_2 H_1^* y_B b_R\right) + m_{V,Q}\bar{Q}_{3,L}V_R\\
&\quad + \bar{V}'_L\left(H_2 y'_T t_R + i\tau_2 H_2^* y'_B b_R\right)\\
&\quad + \sum_{i,j=1}^{2}\bar{Q}_{i,L}\left[H_1(y_u)_{ij}u_{j,R} + i\tau_2 H_1^*(y_d)_{ij}d_{j,R}\right] + h.c.\,,\\
-\mathcal{L}_L &\supseteq \bar{L}_{3,L}\left(H_2 y_{\nu_\tau}\nu_{\tau,R} + i\tau_2 H_2^* y_\tau \tau_R\right) + \bar{\tilde{V}}_L\left(H_1 y_N \nu_{\tau,R} + i\tau_2 H_1^* y_E \tau_R\right) + m_{V,L}\bar{L}_{3,L}\tilde{V}_R\\
&\quad + \bar{\tilde{V}}'_L\left(H_2 y'_N \nu_{\tau,R} + i\tau_2 H_2^* y'_E \tau_R\right)\\
&\quad + \sum_{i,j=1}^{2}\bar{L}_{i,L}\left[H_1(y_\nu)_{ij}\nu_{j,R} + i\tau_2 H_1^*(y_l)_{ij}e_{j,R}\right] + h.c.\,,
\end{aligned}$$

where $V(\Phi)$ represents the potential of the field Φ, $V(H_1, H_2)$ corresponds to the potential of a general two Higgs doublet model, y_α with $\alpha = t, b, \cdots$ and y'_β with $\beta = T, B, N, E$ are Yukawa coupling coefficients, and $m_{V,Q}$ and $m_{V,L}$ are dimensionful parameters. The general form of $V(\Phi)$ is given by [23]

$$\begin{aligned}
V(\Phi) &= -\mu_1^2 Tr(\Phi^\dagger\Phi) - \mu_2^2\left[Tr(\tilde{\Phi}\Phi^\dagger) + Tr(\tilde{\Phi}^\dagger\Phi)\right] + \lambda_1\left[Tr(\Phi^\dagger\Phi)\right]^2\\
&\quad + \lambda_2\left[Tr(\Phi^\dagger\tilde{\Phi})Tr(\tilde{\Phi}^\dagger\Phi)\right] + \lambda_3\left(\left[Tr(\Phi^\dagger\tilde{\Phi})\right]^2 + \left[Tr(\tilde{\Phi}^\dagger\Phi)\right]^2\right)\\
&\quad + \lambda_4\left(Tr(\Phi^\dagger\Phi)\left[Tr(\tilde{\Phi}\Phi^\dagger) + Tr(\tilde{\Phi}^\dagger\Phi)\right]\right) \qquad (2.4)
\end{aligned}$$

with $\tilde{\Phi} = \sigma_2\Phi^*\sigma_2$.

About the Lagrangian in Eq. (2.3), three points should be noted. First, just like the Higgs field in the SM, the filed Φ is responsible not only for symmetry breaking, but also for generating the masses for the vector-like fermions. We emphasize that we introduce the minimal number of the vector-like quark fields to realize the seesaw mechanism for the fermion masses. Second, since the field Φ may have a different dynamical origin from the fields H_1 and H_2, we neglect for simplicity the couplings between Φ and H_i $(i = 1, 2)$ in writing down the scalar potential. These couplings should be small since they can induce the mixings between the H_i fields and Φ, and consequently alter the measured properties of the SM-like Higgs boson. Moreover, if the mixings are switched on, the particle X may decay into the SM-like Higgs pair, and the search for di-Higgs signal at the LHC Run-I has also required the couplings to be small [13]. Third, the third generation fermions in our model can in principle mix with the vector-like quarks. If any of the coefficients y_β, y'_β and m_V is large, the flavor mixings of the fermions in the model may differ greatly from the SM case [22]. Although this situation may still be allowed by the precise measurements in flavor physics, we require all the coefficients to be sufficiently small to suppress the decay of the particle X into the $t\bar{t}$ state. We will turn to this issue later.

In the following, we list the spectrum of the particles that we are interested in.

2.1. Scalar sector

In the topflavor seesaw model, the bi-doublet Higgs field contains 8 real freedoms, and it can parameterized by

$$\Phi = \frac{1}{\sqrt{2}} \begin{pmatrix} \sqrt{2}v + (\rho_1 + i\eta_1) & \sqrt{2}V_1^+ \\ \sqrt{2}V_2^- & \sqrt{2}v + \rho_2 + i\eta_2 \end{pmatrix}, \tag{2.5}$$

where ρ_1 and ρ_2 are CP-even fields with $\sqrt{2}v$ being their common vacuum expectation value, η_1 and η_2 are CP-odd fields, and V_1^+ and V_2^- denote charged fields. The non-zero v triggers the breaking of the group $SU(2)_1 \times SU(2)_2$ into the diagonal $SU(2)_L$ group. In such a process, the field combinations $\eta_1 - \eta_2$ and $V_1^+ - (V_2^-)^*$ act as Goldstone modes, and are absorbed by the gauge bosons of the broken symmetry (denoted by $SU(2)_H$ hereafter). Their orthogonal combinations correspond to physical charged and CP-odd scalars respectively, which are given by

$$H^+ = \frac{1}{\sqrt{2}} \left[V_1^+ + (V_2^-)^* \right], \tag{2.6}$$

$$A^0 = \frac{1}{\sqrt{2}} \left[\eta_1 + \eta_2 \right]. \tag{2.7}$$

As for the CP-even fields ρ_1 and ρ_2, they mix to form mass eigenstates h^0 and H^0 in following way

$$\begin{pmatrix} h^0 \\ H^0 \end{pmatrix} = \frac{1}{\sqrt{2}} \begin{pmatrix} 1 & 1 \\ -1 & 1 \end{pmatrix} \begin{pmatrix} \rho_1 \\ \rho_2 \end{pmatrix}. \tag{2.8}$$

With these physical states, the field Φ can be reexpressed by

$$\Phi \equiv \frac{1}{2} \begin{pmatrix} 2v + h^0 - H^0 + iA^0 & H^+ \\ H^- & 2v + h^0 + H^0 + iA^0 \end{pmatrix}. \tag{2.9}$$

This form is helpful to understand our expansion result of the $V(\Phi)$.

From Eq. (2.4), one can get the minimization condition of the potential, $4\kappa v^2 = \mu_1^2 + 2\mu_2^2$ with $\kappa = \lambda_1 + \lambda_2 + 2\lambda_3 + 2\lambda_4$, and the vacuum stability condition $\kappa > 0, 2(\lambda_1 + \lambda_4)v^2 + \mu_2^2 > 0$. One can also get the spectrum of the scalars as follows

$$m_{h^0}^2 = \mu_1^2 + 2\mu_2^2 = 4\kappa v^2, \tag{2.10}$$

$$m_{H^0}^2 = 2\mu_2^2 - \mu_1^2 + 4(\lambda_1 - \lambda_2 - 2\lambda_3)v^2, \tag{2.11}$$

$$m_{A^0}^2 = 2\mu_2^2 - \mu_1^2 + 4(\lambda_1 + \lambda_2 - 6\lambda_3)v^2, \tag{2.12}$$

$$m_{H^+}^2 = m_{H^0}^2. \tag{2.13}$$

For the potential $V(\Phi)$, one may choose v, m_{h^0}, m_{H^0}, m_{A^0}, λ_4 and $x = 2(\lambda_1 - \lambda_2 - 2\lambda_3)$ as independent input parameters, where the parameter x can be used to parameterize the $h^0 H^+ H^-$ interaction (see Eq. (A.4)). From above argument, one can conclude that if the parameter λ_3 is positively large, A^0 can be significantly lighter than the other scalars. One can also conclude that for positive λ_1, λ_4 and μ_2^2 which can be easily satisfied, the vacuum stability condition becomes the requirement $\kappa > 0$.

In a similar way, the two Higgs doublets H_1 and H_2 can be written as

$$\langle H_i \rangle = \left(H_i^+, \frac{1}{\sqrt{2}}(v_i + H_i^0 + iA_i^0) \right) \tag{2.14}$$

with $v_1^2 + v_2^2 \equiv v_{EW}^2$ and $\tan\beta \equiv v_2/v_1$, and the non-zero v_is break the $SU(2)_L \times U(1)_Y$ gauge symmetry into the $U(1)_Q$ symmetry. In this process, the alignment of the fields H_1^0 and H_2^0 forms a lightest CP-even scalar, which corresponds to the 125 GeV Higgs boson discovered by the ATLAS and CMS Collaborations at the LHC [24,25].

In our model, the particle X may be identified as h^0 and/or A^0. In this case, the Higgs sector for the electroweak symmetry breaking acts as a spectator of the excess, and consequently the electroweak vacuum is unaffected by the diphoton excess. This is different from the situation of the minimal framework discussed in [14]. In the following, we only need to discuss the stability of the vacuum for the potential $V(\Phi)$.

2.2. Gauge bosons

In our theory, the covariant derivative that appears in the kinetic term of Φ is given by

$$D_\mu \equiv \partial_\mu - i\bar{g}_2 W_{1,\mu}^a (T_1^a) + i\tilde{g}_2 W_{2,\mu}^b (T_2^b) + i g_Y Y B_\mu \,, \tag{2.15}$$

where T_1^a and T_2^b with $a, b = 1, 2, 3$ are the $SU(2)$ generators, Y is the hypercharge generator, and $\bar{g}_2$, $\tilde{g}_2$ and g_Y are gauge coupling coefficients. After the first step symmetry breaking, the $SU(2)_L$ coupling coefficient g_2 is related with $\bar{g}_2$ and $\tilde{g}_2$ by

$$\frac{1}{g_2^2} = \frac{1}{\bar{g}_2^2} + \frac{1}{\tilde{g}_2^2} \,, \tag{2.16}$$

which implies $\bar{g}_2 = g_2/\cos\theta$, $\tilde{g}_2 = g_2/\sin\theta$ with $\tan\theta \equiv \bar{g}_2/\tilde{g}_2$, and the gauge fields corresponding to the broken generators (usually called flavorons and denoted by F_μ^i hereafter) and the $SU(2)_L$ group (denoted by W_μ^i) are

$$\begin{pmatrix} F_\mu^i \\ W_\mu^i \end{pmatrix} = \begin{pmatrix} \sin\theta & \cos\theta \\ -\cos\theta & \sin\theta \end{pmatrix} \begin{pmatrix} W_{1,\mu}^i \\ W_{2,\mu}^i \end{pmatrix}, \tag{2.17}$$

with $i = \pm, 3$. At this stage, the fields $F_\mu^\pm$ and F_μ^3 are degenerated in mass and their common squared mass is $m_{F_\mu^i}^2 = (\bar{g}_2^2 + \tilde{g}_2^2)v^2 = 4g_2^2 v^2(\csc^2 2\theta)$. By contrast all the fields W_μ^i keep massless.

After the second step symmetry breaking, the masses of the fields $F_\mu^\pm$ keep unchanged, but the field F_μ^3 mixes with the other neutral gauge fields to form mass eigenstates. In the basis $(F_\mu^3, W_\mu^3, B_\mu)$, the squared mass matrix is given by

$$\frac{h^2}{4} \begin{pmatrix} 4v^2 + s_\theta^4 v_1^2 + c_\theta^4 v_2^2 & s_\theta c_\theta (s_\theta^2 v_1^2 - c_\theta^2 v_2^2) & -\frac{g_Y}{4h}(s_\theta^2 v_1^2 - c_\theta^2 v_2^2) \\ s_\theta c_\theta (s_\theta^2 v_1^2 - c_\theta^2 v_2^2) & s_\theta^2 c_\theta^2 v_{EW}^2 & -\frac{g_Y}{h} s_\theta c_\theta v_{EW}^2 \\ -\frac{g_Y}{4h}(s_\theta^2 v_1^2 - c_\theta^2 v_2^2) & -\frac{g_Y}{h} s_\theta c_\theta v_{EW}^2 & \frac{g_Y^2}{h^2} v_{EW}^2 \end{pmatrix}, \tag{2.18}$$

where $h = \sqrt{\bar{g}_2^2 + \tilde{g}_2^2}$, $s_\theta \equiv \sin\theta$ and $c_\theta \equiv \cos\theta$. This matrix can be diagonalized by a rotation matrix U to get mass eigenstates (Z', Z, γ). Consequently we have

$$\left(Z' \,, Z \,, \gamma\right) = \left(F_\mu^3 \,, W_\mu^3 \,, B_\mu\right) U^T \,. \tag{2.19}$$

2.3. Heavy fermions

After the first step gauge symmetry breaking, the mass matrix for the vector-like quarks V and V' is given by

$$(\bar{V}_L\ ,\ \bar{V}'_L)\begin{pmatrix}\lambda_V v\hat{1} & M_H\hat{1}\\ M_H\hat{1} & \lambda_V v\hat{1}\end{pmatrix}\begin{pmatrix}V_R\\ V'_R\end{pmatrix}+h.c., \tag{2.20}$$

where $\hat{1}$ denotes a 2×2 unit matrix. The corresponding mass eigenstates are given by the combinations

$$Q^1_{L,R}=\frac{1}{\sqrt{2}}\left(V_{L,R}-V'_{L,R}\right)\equiv(\mathcal{T}^1,\mathcal{B}^1)_{L,R}, \tag{2.21}$$

$$Q^2_{L,R}=\frac{1}{\sqrt{2}}\left(V_{L,R}+V'_{L,R}\right)\equiv(\mathcal{T}^2,\mathcal{B}^2)_{L,R}, \tag{2.22}$$

and their masses are $M_{\mathcal{T}^1}=M_{\mathcal{B}^1}=\lambda_V v-M_H$ and $M_{\mathcal{T}^2}=M_{\mathcal{B}^2}=\lambda_V v+M_H$.

In the basis $(t,\mathcal{T}^1,\mathcal{T}^2)$, the mass matrix of the heavy up-type quarks at the weak scale is given by[1]

$$\left(\bar{t}_L\ \ \bar{\mathcal{T}}^1_L\ \ \bar{\mathcal{T}}^2_L\right)\begin{pmatrix}y_t v_2 & \frac{1}{\sqrt{2}}m_V & \frac{1}{\sqrt{2}}m_V\\ \frac{1}{\sqrt{2}}(y_T v_1-y'_T v_2) & \lambda_V v-M_H & 0\\ \frac{1}{\sqrt{2}}(y_T v_1+y'_T v_2) & 0 & \lambda_V v+M_H\end{pmatrix}\begin{pmatrix}t_R\\ \mathcal{T}^1_R\\ \mathcal{T}^2_R\end{pmatrix}. \tag{2.23}$$

This matrix can be diagonalized to get the mass eigenstates (t_1,t_2,t_3). Since we are interested in the case that $y_t v_2, m_V, (y_T v_1\pm y'_T v_2)\ll\lambda_V v-M_H<\lambda_V v+M_H$, the mass eigenstate t_2 is dominated by the field $\mathcal{T}^1$ with $m_{t_2}\simeq\lambda_V v-M_H$, and similarly t_3 is dominated by the field $\mathcal{T}^2$ with $m_{t_3}\simeq\lambda_V v+M_H$. For this case, we note that the seesaw mechanism is mainly responsible for the mass splitting among the vector-like fermions, and it has little to do with top quark mass generation. This situation, although we still dub it as the topflavor seesaw model, differs from the original one proposed in [22] where the seesaw mechanism was fully responsible for top quark mass generation.

About the heavy up-type quarks, two points should be clarified. One is that the mixings between t and $\mathcal{T}^i$ can induce $h^0\bar{t}_1 t_1$ and $A^0\bar{t}_1 t_1$ interactions with t_1 corresponding to top quark discovered at Tevatron, and consequently the upper bound on the process $pp\to X\to t\bar{t}$ from the LHC Run-I data, $\sigma^{8\ \text{TeV}}_{m_X=750\ \text{GeV}}\leq 450$ fb [26], has required the mixings to be moderately small in our explanation of the excess. This fact in return implies that the effect of the mixings on top quark mass is less important. Numerically speaking, for the typical parameters $\lambda_V=4$, $v=5$ TeV and $\lambda_V V-m_H=1$ TeV which are needed to explain the diphoton excess (see following discussion about Fig. 2), we find that top quark mass is predicted to be less than about 15 GeV if y_t or v_2 is set zero. So in order to get the right top quark mass, the field H_2 has to be introduced to generate the bulk of the mass by its Yukawa coupling.[2] The other point is that in our following discussion of the diphoton excess, we assume for simplicity the mixings to be

[1] In order to simplify our discussion, we do not consider the small mixings between the third generation fermions and the first two generations.

[2] We remind that due to the transform properties of top quark and H_1 under the gauge group, there is no $H_1 t\bar{t}$ Yukawa coupling in our model.

sufficiently small so that $Br(h^0/A^0 \to gg) \gg Br(h^0/A^0 \to t\bar{t})$. In this case, the contribution of $h^0/A^0 \to t_1\bar{t}_1$ to the total width of h^0/A^0 can be safely neglected. We remind that even though the mixings are small, they are still able to induce the prompt decays of $t_{2,3}$ like $t_{2,3} \to Wb, t_1 Z$, and the LHC searches for vector-like fermions have required $m_{t_{2,3}} \gtrsim 800$ GeV [27].

In a similar way, one can discuss the characters of the down-type quarks and leptons. A minor difference from the heavy up-type quarks comes from the fact that the seesaw mechanism may be fully responsible for bottom or τ mass after considering the relevant constraints from the LHC Run-I. So it is fair to say that in our model, the seesaw mechanism is responsible not only for potentially large mass splitting among the vector-like fermions, but also for the partial or full mass generation for the third family fermions.

3. The diphoton excess

If the diphoton excess observed by both ATLAS and CMS Collaborations is initiated by gluon fusion, its production rate can be written as [13,28]

$$\begin{aligned}\sigma^{\gamma\gamma}_{13\ \mathrm{TeV}}(pp \to \gamma\gamma) &= \sum_i \sigma^{\gamma\gamma}_{13\ \mathrm{TeV}}(pp \to \phi_i \to \gamma\gamma) \\ &= \sum_i \frac{\Gamma_{\phi_i \to gg}}{\Gamma^{SM}_{H\to gg}}|_{m_H \simeq 750\ \mathrm{GeV}} \times \sigma^{SM}_{\sqrt{s}=13\ \mathrm{TeV}}(H) \times Br(\phi_i \to \gamma\gamma), \quad (3.1)\end{aligned}$$

where ϕ_i may be h^0 and/or A^0 in our model, H denotes the Higgs boson in the SM satisfying $m_H = 750$ GeV, $\Gamma_{\phi_i \to gg}$ and $\Gamma^{SM}_{H\to gg} = 6.22 \times 10^{-2}$ GeV are the widths of $\phi_i \to gg$ and $H \to gg$ respectively, and $\sigma^{SM}_{\sqrt{s}=13\ \mathrm{TeV}}(H) = 735$ fb represents the NNLO H production rate at the 13 TeV LHC [29]. As pointed out in [3], after combining the diphoton data at the 13 TeV LHC with those at the 8 TeV LHC, the preferred rate for the excess at the 13 TeV LHC is

$$\sigma^{\gamma\gamma}_{13\ \mathrm{TeV}}(pp \to \gamma\gamma) = (4.6 \pm 1.2)\ \mathrm{fb}. \quad (3.2)$$

This rate can be translated into the requirement

$$\sum_i \frac{\Gamma_{\phi_i \to gg}}{\Gamma_{\phi_i, tot}} \times \Gamma_{\phi_i \to \gamma\gamma} = (3.9 \pm 1.0) \times 10^{-4}\ \mathrm{GeV}, \quad (3.3)$$

where $\Gamma_{\phi_i, tot}$ denotes the total width of ϕ_i, and in our model it is given by

$$\Gamma_{\phi_i, tot} = \Gamma_{\phi_i \to gg} + \Gamma_{\phi_i \to \gamma\gamma} + \Gamma_{\phi_i \to Z\gamma} + \Gamma_{\phi_i \to W^+W^-} + \Gamma_{\phi_i \to ZZ}. \quad (3.4)$$

In the appendix of this work, we present the calculation of the partial widthes appeared on the right side of Eq. (3.4), and the final results are summarized in Eq. (B.9) for $\phi_i = h^0$ case after neglecting W and Z masses. From the formulae in Eq. (B.9), one can infer that if these decays are induced mainly by the vector-like fermions (which is the case in our model to explain the excess, see discussion below), the decay mode $\phi_i \to gg$ will be dominant. Eq. (3.3) is then approximated by

$$\sum_i \Gamma_{\phi_i \to \gamma\gamma} \simeq (3.9 \pm 1.0) \times 10^{-4}\ \mathrm{GeV}. \quad (3.5)$$

In our discussion, we will use this approximation to estimate the favored parameter space for the diphoton excess. The formulae in Eq. (B.9) also indicate that the branching ratios for the

decays $\phi_i \to W^+W^-, ZZ, Z\gamma$ are usually at least several times larger than that of $\phi_i \to \gamma\gamma$. As a result, the ϕ_i production can also generate sizable W^+W^-, ZZ and $Z\gamma$ signals. Considering that the LHC Run I has imposed upper bounds on these channels, which are given by [13]

$$\sigma_{8\ \mathrm{TeV}}(pp \to X \to Z\gamma) \leq 3.6\ \mathrm{fb}, \quad \sigma_{8\ \mathrm{TeV}}(pp \to X \to ZZ) \leq 12\ \mathrm{fb},$$
$$\sigma_{8\ \mathrm{TeV}}(pp \to X \to W^+W^-) \leq 37\ \mathrm{fb}, \quad \sigma_{8\ \mathrm{TeV}}(pp \to X \to gg) \leq 1.8\ \mathrm{pb}, \tag{3.6}$$

for $m_X = 750$ GeV, we will use these channels to constrain the parameter space of our model.

In the following, we interpret the diphoton excess by taking either $m_{h^0} \simeq 750$ GeV or $m_{A^0} \simeq 750$ GeV. We also briefly discuss the case that both h^0 and A^0 contribute to the excess.

3.1. h^0 acting as the 750 GeV resonance state

In this case, the flavorons, the vector-like fermions as well as the scalar H^+ contribute to the $h^0\gamma\gamma$ interaction through their loop effects. From the formulae in Eq. (B.9), one can learn that the involved parameters for the diphoton signal are

- the parameters in the scalar sector, which are $m_{h^0} = 750$ GeV, v, x and $m_{H^+} = m_{H^0}$.
- the parameter $\tan\theta$ in the gauge sector, which determines the flavoron masses.
- the parameters in the fermion sector, which are λ_V and m_H used to determine the fermion masses and their Yukawa couplings.

In order to illustrate our explanation of the excess in a concise way, we assume that the intermediate particles in the loops are significantly heavier than h^0. Then by using Eq. (B.4) and Eq. (B.9), one can simplify Eq. (3.5) as follows

$$|\frac{-7}{v} + \frac{8}{3}(\frac{\lambda_V}{\lambda_V v - m_H} + \frac{\lambda_V}{\lambda_V v + m_H})\frac{4}{3} + \frac{x}{3v}| \simeq \frac{20.7 \pm 2.8}{\mathrm{TeV}}. \tag{3.7}$$

This equation reveals the following information

- The contribution from the flavorons interferes destructively with the fermion contribution. While for the scalar contribution, it may interfere either constructively (for $x > 0$) or destructively (for $x < 0$) with the fermion contribution.
- If $m_H \simeq 0$, the contribution from each of the vector-like fermions is usually significantly smaller than the vector boson contribution, but the total fermion contribution in our model can cancel strongly with the vector contribution regardless the value of λ_V. On the other hand, if m_H is sufficiently large so that $\lambda_V v - m_H \ll \lambda_V v$ or equally speaking $\lambda_V/(\lambda_V v - m_H) \gg 1/v$, the fermion contribution may be dominant. This guides us to obtain the solution for the diphoton excess.
- For $x \sim 1$, the scalar contribution is very small in comparison with the other contributions. However, if $|x| \gg 1$ which is somewhat unnatural but still possible by tuning μ_1^2 and μ_2^2 to get $m_{H^+}^2$ in Eq. (2.13), the scalar contribution can be important.
- For a large v, the contributions from the flavorons and the scalar H^+ decrease quickly since they are proportional to $1/v^2$. By contrast, if one keeps the lighter vector-like fermions at TeV scale by requiring $(\lambda_V v - m_H) \sim 1$ TeV, the vector-like fermion contribution can still be sizable even for a very large v. In this case, the effective theory of our model at TeV scale is quite similar to the minimal model mentioned in section 1.

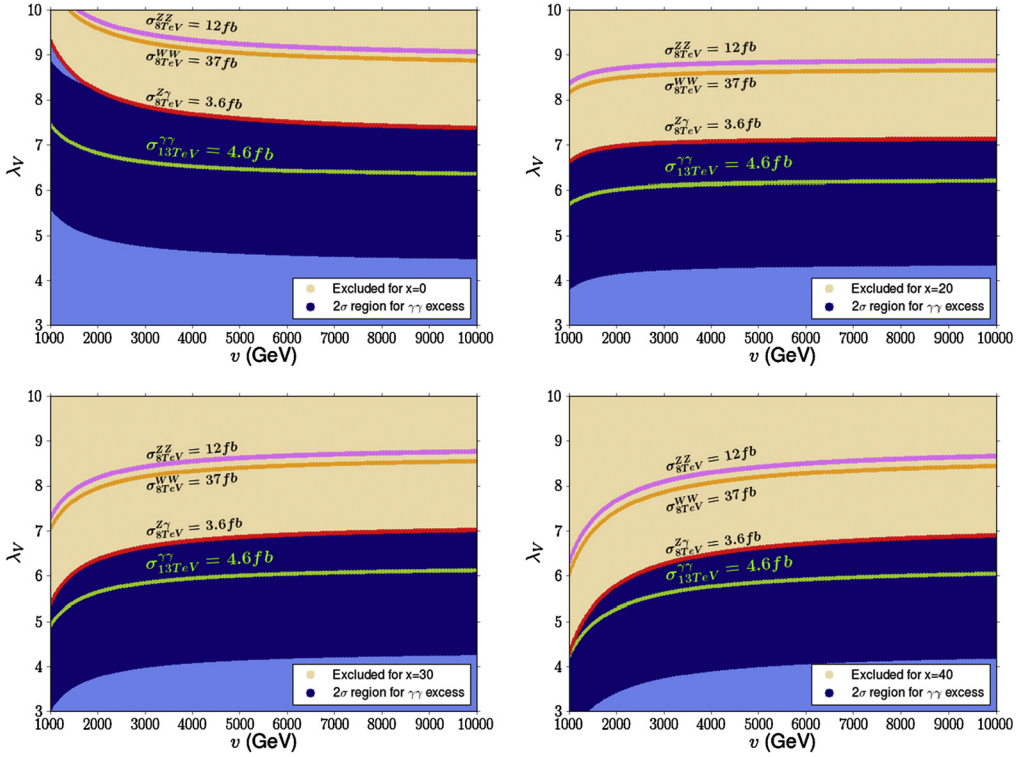

Fig. 1. Favored parameter space on the $\lambda_V - v$ planes for the diphoton excess with different choices of x, which parameterizes the $h^0H^+H^-$ and $h^0H^0H^0$ couplings. The regions shaded by the blue color are able to explain the excess at 2σ level, and by contrast the regions covered by straw color are excluded by the upper bounds on $Z\gamma$ signal at the LHC Run I. The blue lines correspond to $\sigma^{\gamma\gamma}_{13\text{ TeV}} = 4.4$ fb, which is the central value for the diphoton excess, and the red lines, brown yellow lines and pink lines are the boundary lines of the $Z\gamma$, W^+W^- and ZZ signals at the 8 TeV LHC respectively. In getting this figure, we fix the masses of the lighter vector-like fermions at 1 TeV (i.e. $m_{F_1} = \lambda_V v - m_H = 1$ TeV), $m_{H^+} = m_{H^0} = v$, and assume that only h^0 is responsible for the excess. In this case, the effective theory of our model at 1 TeV contains only the vector-like fermions and h^0 for a sufficiently large v. Note that the Yukawa coupling coefficient for the $h^0\bar{F}F$ interaction is $\lambda_V/2$, instead of λ_V. (For interpretation of the references to color in this figure legend, the reader is referred to the web version of this article.)

- For $v = 10$ TeV, $\lambda_V - m_H = 1$ TeV and $x = 0$, one can estimate by Eq. (3.7) that $\lambda_V \simeq 6.3 \pm 0.9$ can explain the diphoton excess at 1σ level. The corresponding Yukawa coefficient for the $h^0\bar{t}_2 t_2$ interaction is about 3.1 ± 0.4, which is roughly 3 times the top quark Yukawa coupling. It is quite large, but still below the perturbative bound $\sqrt{4\pi}$.

Throughout our discussion in this work, we fix $\tan\theta = 1$, $m_{H^+} = m_{H^0} = v$, and $\lambda_V v - m_H = 1$ TeV. In studying the h^0 explanation of the excess, we fix $m_{h^0} = 750$ GeV, and vary λ_V and v to get the favored parameter region with $x = 0, 20, 30, 40$ at each time. The contours of $\sigma^{Z\gamma}_{8\text{ TeV}} = 3.6$ fb, $\sigma^{ZZ}_{8\text{ TeV}} = 12$ fb and $\sigma^{WW^*}_{8\text{ TeV}} = 37$ fb in the $\lambda_v - v$ plane are also plotted. The corresponding results are shown in Fig. 1, where the upper panels are for the results with $x = 0, 20$ respectively and the lower panels correspond to the results with $x = 30, 40$ respectively. From this figure, one can get following conclusions

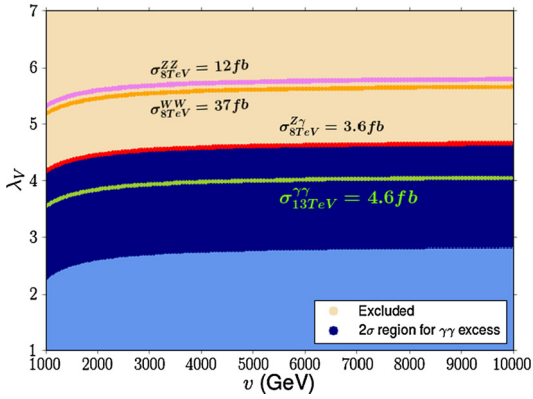

Fig. 2. Same as Fig. 1, but for the case that only A^0 is responsible for the diphoton excess.

- The topflavor seesaw model can explain the diphoton excess without conflicting with the constraints from the data at the LHC Run I, and the central value of the excess can be obtained even for $v \sim 10$ TeV.
- Given a sufficiently large v, e.g. $v \gtrsim 6$ TeV, $\lambda_V \simeq 6$ is needed to predict the central value of the excess. In this case, the corresponding $h^0\bar{t}_2 t_2$ Yukawa coupling is about 3.
- For $v \simeq 1$ TeV and $x = 40$, which corresponds to a tuning of $1/x$ in getting the squared mass of H^+, $\lambda_V \simeq 4$ is able to predict the central value of the excess. Especially, we note that λ_V as low as 2.5 is capable to explain the excess at 2σ level.
- The LHC data at Run I have imposed rather tight constraints on our model. For the field configurations in our theory, the strongest constraint comes from the upper bound on the $Z\gamma$ channel $\sigma^{Z\gamma}_{8\ \mathrm{TeV}} \lesssim 3.6$ fb, and it has required $\sigma^{\gamma\gamma}_{13\ \mathrm{TeV}} \lesssim 6$ fb. Alternatively, if one use $\sigma^{Z\gamma}_{8\ \mathrm{TeV}} \lesssim 6$ fb adopted in [3] as the constraint, we find that $\sigma^{\gamma\gamma}_{13\ \mathrm{TeV}}$ may reach about 10 fb.
- We emphasize that the perturbative bound $\lambda_V \lesssim \sqrt{4\pi}$ may be stronger than the $Z\gamma$ channel in constraining the parameter space that we are interested in.

3.2. A^0 acting as the 750 GeV resonance state

In the case that A^0 acts as the 750 GeV resonance state, only the vector-like fermions contribute to the $A^0\gamma\gamma$ interaction. On condition that the fermions are significantly heavier than 750 GeV, Eq. (3.5) can be rewritten as

$$\left|\frac{8}{3}\left(\frac{\lambda_V}{\lambda_V v - m_H} + \frac{\lambda_V}{\lambda_V v + m_H}\right) \times 2\right| \simeq \frac{20.7 \pm 2.8}{\mathrm{TeV}}, \tag{3.8}$$

where we have used Eq. (B.10) and Eq. (B.12) for the expression of $\Gamma_{A^0\to\gamma\gamma}$. Compared with Eq. (3.7) for the $m_{h^0} \simeq 750$ GeV case, Eq. (3.8) indicates that the A^0 explanation usually needs a smaller λ_V for the excess because the involved loop functions satisfy $A^A_{\frac{1}{2}}(\tau_F) > A_{\frac{1}{2}}(\tau_F)$ in large τ_F limit, and also because there is no cancelation between the vector boson contribution and the fermion contribution.

In Fig. 2, we show the favored parameter space for the excess if only A^0 is responsible for the diphoton excess. This figure indicates that in order to get the central value of the excess,

$\lambda_V \simeq 4$ is preferred for $v \geq 2$ TeV, and among the constraints the tightest one comes from the $Z\gamma$ channel at the LHC Run I, which is quite similar to the h^0 explanation.

We emphasize that in the A^0 explanation, one may choose a sufficient large $\kappa \equiv \lambda_1 + \lambda_2 + 2\lambda_3 + 2\lambda_4 = m^2_{h^0}/v^2$ (corresponding to a heavy h^0) as an input parameter. In this case, the contributions of the bi-doublet scalar particles to the β functions of the coefficients λ_is in $V(\Phi)$ can be positively large to cancel the negative contributions of the vector-like fermions. As a result, $\kappa > 0$ can always be satisfied in the RGE evolution of the λ_is to guarantee the stability of $V(\Phi)$ vacuum.[3] By contrast, in the h^0 explanation, κ is equal to $750^2/v^2$ and approaches zero for a large v. In this case, one must carefully choose the input parameters of the theory to keep the vacuum stable in the renormalization group running. Since the vacuum stability of $V(\Phi)$ involves many independent parameters such as λ_i with $i = 1, 2, 3, 4$ and various Yukawa couplings, we do not investigate such an issue in detail. Instead, we consider the Landau pole problem related to the Yukawa couplings of the vector-like fermions. In Appendix C we present one loop renormalization group equations (RGE) for all the Yukawa couplings in Eq. (2.3). From the first four equations of them, we roughly estimate the running of the Yukawa couplings for the vector-like fermions by neglecting the contributions from gauge couplings and the other Yukawa couplings, and also by assuming $y^{\Phi}_V \simeq y^{\Phi}_{V'} \simeq y^{\tilde{\Phi}}_V \simeq y^{\tilde{\Phi}}_{V'}$ in the RGE running. We find that for $\lambda_V = 4$, $v = 5$ TeV at the renormalization scale $\mu = 1$ TeV, the Yukawa couplings will not reach its Landau pole below the scale 100 TeV.

We also study the case that both h^0 and A^0 contribute to the diphoton excess. The corresponding favored parameter regions for the excess are shown in Fig. 3. This figure is somewhat similar to Fig. 1, and the main difference is that λ_V usually takes a lower value to predict the central value of the excess. The underlying reason is that in explaining the excess, h^0 only needs to provide a part contribution to the diphoton events since A^0 also contributes to the signal. About Fig. 1–3, we emphasize that they are obtained by fixing the lighter vector-like fermions at 1 TeV. If a lower common mass of the fermions is chosen, a decreased λ_V is enough to explain the excess.

Before we end this section, we point out that there are two ways to test our explanations in future LHC experiments. One is that in our explanations, all the decay modes of h^0 and A^0 proceed through loop effects which are mainly mediated by the vector-like fermions. As a result, the rates of these decays are correlated. For example, in the explanation with $m_{A^0} \simeq 750$ GeV we find that $\Gamma_{A^0\to\gamma\gamma} : \Gamma_{A^0\to gg} : \Gamma_{A^0\to Z\gamma} : \Gamma_{A^0\to ZZ} : \Gamma_{A^0\to W^+W^-} \simeq 1 : 204 : 3.1 : 6.9 : 21.8$, and as to the h^0 explanation, this correlation also holds for the parameter points in the blue lines of Fig. 1 and meanwhile satisfying $v \gtrsim 5$ TeV. This fact implies that sizable $Z\gamma$, W^+W^- and ZZ signals are companied with the diphoton excess, and looking for them at the future LHC can verify our

[3] Generally speaking, the contributions of scalar particles to the β functions of the quartic couplings λ_i are positive if $\lambda_i > 0$, while those of fermions are negative [30]. In the minimal framework, $\lambda_F = m_F/v_S$ if the interaction $\lambda_F S\bar{F}F$ is fully responsible for m_F. The condition of vacuum stability is $4\lambda_H\lambda_S - \lambda^2_{HS} > 0$ for the scalar potential $V(H, S) = \lambda_H|H|^4 + \frac{\lambda_{HS}}{2}|H|^2S^2 + \frac{\lambda_S}{4}S^4$ [14]. To explain the diphoton excess, $\lambda_S \simeq (750\ \text{GeV})^2/(2v^2_S)$ with v_S determined by the diphoton rate and the electric charge of F [14]. The value of λ_S at the renormalization scale $\mu \simeq 750$ GeV, which acts as the initial input of the RGE, is tightly limited. Especially, it is correlated with λ_F by $\lambda^2_F/\lambda_S \simeq 2m^2_F/(750\ \text{GeV})^2$ for a given m_F (note that m_F and $\lambda_F = m_F/v_S$ are also the inputs of the RGE running). As a result, the negative contribution of λ_F to the β function always pushes λ_S to be negative for $m_F \sim 1$ TeV so that the vacuum becomes unstable [14]. In our model, however, λ_i and λ_V as the input of the RGEs are independent even though the low energy effective theory is similar to the minimal framework, and this brings us more freedom in choosing their values to keep $\kappa > 0$ in the RGE running.

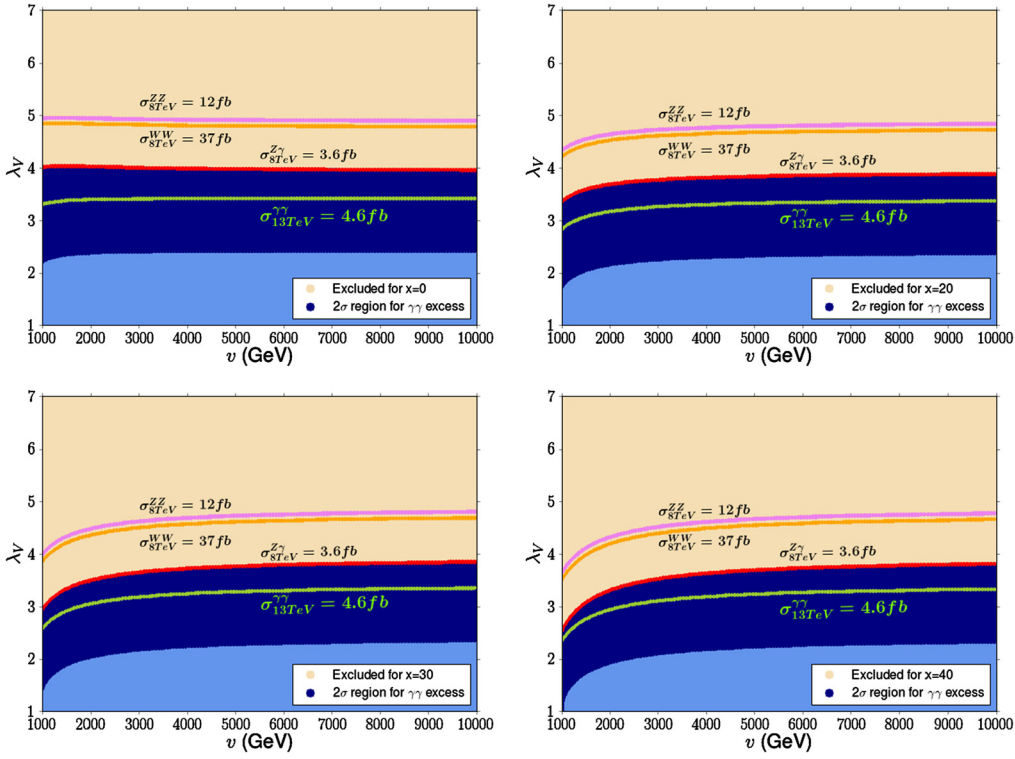

Fig. 3. Same as Fig. 1, but for both h^0 and A^0 responsible for the diphoton excess.

explanation (we note that studies in this direction was recently emphasized in [31]). The other way is that in our explanation, the diphoton rate is mainly determined by the rate $\lambda_V/(\lambda_V v - M_H)$ for a large v, where $\lambda_V v - M_H$ represents the mass of lighter vector-like fermions. So for $\frac{\lambda_V}{2} \lesssim 3$ which is favored by the perturbativity of the Yukawa couplings, the fermions can not be too heavy. As a result, the t_2 pair production process at the LHC with $t_2 \to tZ, bW$ or the b_2 pair production process with $b_2 \to tW, bZ$ may be detectable in future new physics searches.

4. Conclusion

In this work, we proposed to interpret the 750 GeV diphoton excess in a typical topflavor seesaw model. In our scheme, the new resonance X is identified as a CP-even or CP-odd scalar emerging from a certain bi-doublet Higgs field, and it may couple rather strongly with the vector-like fermions, charged scalars as well as heavy gauge bosons introduced in the model. These new particles in return can induce sizable $X\gamma\gamma$ and Xgg couplings, which makes it possible for the model to explain the diphoton excess in reasonable parameter regions. Numerical analysis indicates that the model can predict the central value of the diphoton excess without contradicting any constraints from 8 TeV LHC, and among the constraints, the tightest one comes from the upper bound on the $Z\gamma$ channel, $\sigma^{Z\gamma}_{8\text{ TeV}} \lesssim 3.6$ fb, which requires $\sigma^{\gamma\gamma}_{13\text{ TeV}} \lesssim 6$ fb in most of the favored parameter space. The phenomenology and some theoretical issues such as vacuum stability and Landau pole of the involved Yukawa couplings in explaining the excess are also addressed.

We emphasize that there are at least three advantages of our model over the minimal framework in explaining the excess. First, as we mentioned in section 1, the key factor λ_F/M_F for the diphoton rate in the minimal model is equal to $1/v$. As a result, in order to explain the excess v should be as low as possible, which implies that the scale of the new physics behind the excess is not high. While in our model the factor λ_F/M_F is much larger than $1/v$ since we propose a typical seesaw mechanism to generate an effective negative contribution to M_F so that the simple relation $M_F = \lambda_F v$ is unleashed. Consequently a large v is still able to explain the excess. We remind that in the minimal model imposing a negative contribution to M_F by hand lacks physical motivation, and that we introduce the minimal extension of the matter fields to realize the seesaw mechanism. Second, in our explanation the resonance X is naturally embedded in a scalar sector which, just like the Higgs sector in the SM, is responsible not only for the symmetry breaking, but also for generating new particle masses. In the minimal framework, however, the particle X is imposed by hand. Third, in our model we take the A^0 explanation as an example to briefly exhibit that the vacuum stability can not be spoiled by the large Yukawa couplings needed for the explanation. This, on the other hand, is an important problem of the minimal framework [14].

Note added: When we finished this manuscript at the end of 2015, we noted that some gauge group extensions of the SM had been considered to explain the excess [15]. For this type of explanations, the 750 GeV resonance comes from the scalar sector responsible for symmetry breaking, and is thus well motivated. Our work differs from these works mainly in following three aspects. First, previous literatures usually adopted a new $U(1)$ or $SU(3)_L$ group to extend the SM electroweak sector, while we were motivated by the relatively large masses of the third generation fermions in the SM, and took a $SU(2)_1 \bigotimes SU(2)_2$ group. Second, in previous literatures the resonance was usually identified as a CP-even scalar which is responsible for the symmetry breaking. By contrast, in our explanation the resonance may correspond to a CP-odd scalar. Third, we incorporated seesaw mechanism in our model building to split the vector-like fermion masses, and consequently the minimal framework can be recovered from our model at the TeV scale. While in previous literatures, they simply introduced vector-like fermions to mediate the $X\gamma\gamma$ and Xgg interactions.

We also noted that, in the very recent Conference "ICHEP 2016", both ATLAS and CMS Collaborations released their new analyses of the diphoton signal based on the combined 13 TeV data collected in 2015 and in 2016 [32,33]. These analyses indicate that the significance of the excess has reduced to below 2σ. Confronted with such a situation, we have following comments on our model:

- Since the updated 95% upper bounds on the diphoton rate are about 1.5 fb for ATLAS analysis [32] and 2 fb for CMS analysis [33], the Yukawa coupling λ_V is no longer needed to be large. In this case, our theory becomes more safer from the vacuum stability and Landau pole problems, so the validity UV-cutoff of our theory can be extrapolate to much higher scale.
- Our model may be used to explain other diphoton excess observed at the LHC. For example, a diphoton excess with 2.4σ local significance at $m_{\gamma\gamma} \simeq 1.6$ TeV was recently reported by ATLAS Collaboration [32], and another excess was seen at $m_{\gamma\gamma} \simeq 1.3$ TeV with a local significance of 2.2σ by CMS Collaboration [33].
- Our model is still an useful attempt to speculate the form of new physics. Especially we provided the formulae for the RGE of the Yukawa couplings, and the expressions of $h^0/A^0 \to VV'$ induced by $SU(2)$ doublet vector-like fermions, which may be adopted by others in similar studies.

Acknowledgements

This work was supported by the Natural Science Foundation of China under grant numbers 11105124, 11222548, 90103013, 11275245, 11575053 and 11675147; by the Open Project Program of State Key Laboratory of Theoretical Physics, Institute of Theoretical Physics, Chinese Academy of Sciences, P.R. China (No. Y5KF121CJ1); by the Innovation Talent project of Henan Province under grant number 15HASTIT017; by the Outstanding Young Talent Research Fund of Zhengzhou University under grant number 1421317054.

Appendix A. The couplings needed in our calculation

In the section, we enumerate the couplings needed in our calculation.

A.1. *The couplings of h^0 and A^0*

- The couplings of h^0 to gauge bosons.
  These interactions come from the kinetic term

$$\mathcal{L} \supseteq Tr\left[(D_\mu \Phi)^\dagger (D^\mu \Phi)\right], \tag{A.1}$$

  and consequently, we have

$$\mathcal{L} \supseteq \frac{(h_1^2 + h_2^2)v}{2}(F_\mu^3 F^{\mu 3} + 2F_\mu^+ F^{\mu -})h^0. \tag{A.2}$$

- The couplings of h^0/A^0 to vector-like quarks.
  These couplings are given by

$$\begin{aligned}\mathcal{L} \simeq & -\frac{\lambda_V}{2}\left[h^0(\bar{t}_2 t_2 + \bar{t}_3 t_3 + \bar{b}_2 b_2 + \bar{b}_3 b_3) + H^0(\bar{t}_2 t_3 + \bar{t}_3 t_2 + \bar{b}_2 b_3 + \bar{b}_3 b_2)\right] \\ & - \frac{\lambda_V}{2} i A^0(\bar{t}_2 \gamma_5 t_2 + \bar{t}_3 \gamma_5 t_3 + \bar{b}_2 \gamma_5 b_2 + \bar{b}_3 \gamma_5 b_3).\end{aligned} \tag{A.3}$$

  Note that the vector-like leptons have same Yukawa couplings as the quarks, and the coupling coefficient of the $h^0 \bar{t}_2 t_2$ interaction is $-\frac{\lambda_V}{2}$ instead of $-\lambda_V$.
- The couplings of h^0 to heavy scalars
  These couplings originate from the $V(\Phi)$ presented in Eq. (2.4). After tedious expansion of the $V(\Phi)$, we find that they take following forms

$$\begin{aligned}\mathcal{L} \supseteq & -2(\lambda_1 - \lambda_2 - 2\lambda_3) v h^0 (H^0 H^0 + 2H^+ H^-) \\ \equiv & -x\frac{m_{H^+}^2}{v} h^0 (\frac{1}{2} H^0 H^0 + H^+ H^-),\end{aligned} \tag{A.4}$$

  where in the last step we introduce a dimensionless quantity $x = 2(\lambda_1 - \lambda_2 - 2\lambda_3)$ to parameterize the interactions. From Eq. (2.13), one can learn that $x = 1$ if $2\mu_2^2 = \mu_1^2$, and $x > 1$ ($x < 1$) if $2\mu_2^2 < \mu_1^2$ ($2\mu_2^2 > \mu_1^2$).

A.2. The couplings of W and Z bosons to the heavy scalars

These couplings originate from the kinetic term in Eq. (A.1), and the terms relevant to our discussion are given by

$$\begin{aligned}\mathcal{L} \supset & -ig_2\Big[(\partial^\mu H^-)W^+_\mu H^0 - (\partial^\mu H^0)W^+_\mu H^- + (\partial^\mu H^0)W^-_\mu H^+ - (\partial^\mu H^+)W^-_\mu H^0 \\ & + (\partial^\mu H^-)W^3_\mu H^+ - (\partial^\mu H^+)W^3_\mu H^-\Big] \\ & + \frac{1}{2}g_2^2 g^{\mu\nu}\Big[2(W^3_\mu W^+_\nu H^0 H^- + W^3_\mu W^-_\nu H^0 H^+) \\ & - (W^+_\mu W^+_\nu H^- H^- + W^-_\mu W^-_\nu H^+ H^+) \\ & + 2H^+H^-(W^3_\mu W^3_\nu + W^+_\mu W^-_\nu) + 2W^+_\mu W^-_\nu (H^0)^2\Big]. \end{aligned} \tag{A.5}$$

The corresponding Feynman rules are

- $H^-(p_1) - H^+(p_2) - Z^0_\mu(p_3):$ $\quad -ig_2\cos\theta_W(p_1-p_2)_\mu,$
- $H^-(p_1) - H^+(p_2) - A_\mu(p_3):$ $\quad -ie(p_1-p_2)_\mu,$
- $H^0(p_1) - H^+(p_2) - W^-_\mu(p_3):$ $\quad -ig_2(p_1-p_2)_\mu,$
- $H^0(p_1) - H^-(p_2) - W^+_\mu(p_3):$ $\quad ig_2(p_1-p_2)_\mu,$
- $H^+ - H^- - W^+_\mu - W^-_\nu:$ $\quad ig_2^2 g_{\mu\nu},$
- $H^0 - H^0 - W^+_\mu - W^-_\nu:$ $\quad 2ig_2^2 g_{\mu\nu},$
- $H^+ - H^- - Z_\mu - Z_\nu:$ $\quad 2ig_2^2\cos^2\theta_W g_{\mu\nu},$
- $H^+ - H^- - Z_\mu - A_\nu:$ $\quad 2ig_2^2\sin\theta_W\cos\theta_W g_{\mu\nu},$
- $H^+ - H^- - A_\mu - A_\nu:$ $\quad 2ie^2 g_{\mu\nu}.$

In getting the first four rules, we have defined the direction of the momentum as that pointing to the vertex.

A.3. The couplings of W and Z bosons to the heavy fermions

Denoting F to be any of the fermion fields t_2, t_3, b_2, b_3, τ_2, τ_3, ν_{τ_2}, ν_{τ_3}, we have following Feynman rules for W and Z bosons

- $Z_\mu - F - F:$ $\quad -i\frac{g_2}{\cos\theta_W}\gamma_\mu(T^3_q - Q_q\sin^2\theta_W),$
- $W^+_\mu - t_i - b_j:$ $\quad -i\frac{\sqrt{2}}{2}g_2\delta_{ij}\gamma_\mu,$
- $W^+_\mu - \tau_i - \nu_{\tau_j}:$ $\quad -i\frac{\sqrt{2}}{2}g_2\delta_{ij}\gamma_\mu.$

Moreover, we also find that the coupling of the F^+F^-Z interaction is same as that of the W^+W^-Z interaction in the SM, and the coupling of the $F^+W^-F^3$ interaction differs from that of the W^+W^-Z interaction by a factor of $1/\cos\theta_W$.

Appendix B. Useful formulae for calculation

In this section, we list the formulae for the partial widths of h^0 and A^0, which are used to get the diphoton rate.

B.1. Partial widthes of the scalar h^0

- The widths of $h^0 \to \gamma\gamma, gg$ are given by

$$\Gamma_{h^0\to\gamma\gamma} = \frac{\alpha^2 m_{h^0}^3}{1024\pi^3}\left|I_{\gamma\gamma}^{h^0}\right|^2, \qquad \Gamma_{h^0\to gg} = \frac{\alpha_S^2 m_{h^0}^3}{32\pi^3}\left|I_{gg}^{h^0}\right|^2, \tag{B.1}$$

where $I_{\gamma\gamma}^{h^0}$ and $I_{gg}^{h^0}$ parameterize the $h^0\gamma\gamma$ and $h^0 gg$ interactions, and their general expressions are[4]

$$\begin{aligned} I_{\gamma\gamma}^{h^0} &= \frac{g_{h^0VV}}{m_V^2} N_{c,V} Q_V^2 A_1(\tau_V) - \frac{2g_{h^0FF}}{m_F} N_{c,F} Q_F^2 A_{1/2}(\tau_F) - \frac{g_{h^0SS}}{m_S^2} N_{c,S} Q_S^2 A_0(\tau_S), \\ I_{gg}^{h^0} &= \frac{1}{2}\frac{g_{h^0FF}}{m_F} A_{1/2}\left(\frac{4m_F^2}{m_S^2}\right). \end{aligned} \tag{B.2}$$

Here the coefficient g_{h^0PP} with $P = V, F, S$ represents the coupling of the h^0P^*P interaction with its explicit form given in last section, m_P, $N_{c,P}$ and Q_P are the mass, color number and electric charge of the particle P respectively, and $\tau_P = 4m_P^2/m_{h^0}^2$. The involved loop functions are defined by [34]

$$\begin{aligned} A_1(x) &= -[2 + 3x + 3(2x - x^2) f(x)] , \\ A_{\frac{1}{2}}(x) &= 2x[1 + (1 - x) f(x)] , \\ A_0(x) &= -x(1 - xf(x)) , \\ f(x) &= arcsin^2\left(\frac{1}{\sqrt{x}}\right), \quad x \geq 1, \end{aligned} \tag{B.3}$$

and in the limit $x \to \infty$, we have

$$A_1 \to -7, \qquad A_{\frac{1}{2}} \to \frac{4}{3}, \qquad A_0 \to \frac{1}{3}. \tag{B.4}$$

Obviously, the three terms in $I_{\gamma\gamma}^{h^0}$ correspond to the contributions from vector bosons, fermions and scalars, respectively. In our model, $V = F_\mu^+, F_\mu^-$, $F = t_2, t_3, b_2, b_3, \tau_2, \tau_3$ and $S = H^+, H^-$.

- The width of $h^0 \to Z\gamma$ can be obtained in a similar way to that of $h^0 \to \gamma\gamma$, and it is given by [13]

$$\Gamma_{h^0\to Z\gamma} = \frac{G_F^2 m_W^2 \alpha m_{h^0}^3}{64\pi^4}\left(1 - \frac{m_Z^2}{m_{h^0}^2}\right)^3 \left|I_{Z\gamma}^{h^0}\right|^2, \tag{B.5}$$

[4] We remind that the signs for the second and third terms in the expression of $\Gamma_{h^0\to\gamma\gamma}$ are opposite to those in [34]. This is due to the sign convention, and it does not affect the results in this work.

where

$$I^{h^0}_{Z\gamma} = \frac{m_W}{g_2^2}\left[\frac{g_{h^0VV}g'_{ZVV}}{m_V^2}N_{c,V}Q_V A_1(\tau_V) - \frac{2g_{h^0FF}g'_{ZFF}}{m_F}N_{c,F}Q_F A_{1/2}(\tau_F) - \frac{g_{h^0SS}g'_{ZSS}}{m_S^2}N_{c,S}Q_S A_0(\tau_S)\right] \tag{B.6}$$

with g'_{ZPP} $(P = V, F, S)$ standing for the coefficient of the ZP^*P interaction. Note that in getting this expression, we have neglected the Z boson mass appeared in the loop functions since $m^2_{h^0}, m^2_P \gg m^2_Z$, and consequently the involved loop functions can be greatly simplified.

- In the topflavor seesaw model, the decays $h^0 \to ZZ, W^+W^-$ are also induced by loop effects. Their width expressions are slightly complex, but can be obtained in a way similar to that of $h^0 \to \gamma\gamma$ if one neglects the vector boson masses appeared in the relevant loop functions. Explicitly speaking, we have [13]

$$\Gamma_{h^0\to VV^*} = \delta_V \frac{G_F m^3_{h^0}}{16\pi\sqrt{2}}\frac{4m_V^4}{m^4_{h^0}}\sqrt{\lambda(m_V^2, m_V^2; m^2_{h^0})}\times\left[A_V A_V^*\times\left(2+\frac{(p_1\cdot p_2)^2}{m_V^4}\right) + (A_V B_V^* + A_V^* B_V)\times\left(\frac{(p_1\cdot p_2)^3}{m_V^4} - p_1\cdot p_2\right) + B_V B_V^*\times\left(m_V^4 + \frac{(p_1\cdot p_2)^4}{m_V^4} - 2(p_1\cdot p_2)^2\right)\right], \tag{B.7}$$

where $\delta_V = 2(1)$ for $V = W(Z)$, $\lambda(x, y, z) = ((z - x - y)^2 - 4xy)/z^2$ and $p_1 \cdot p_2 = \frac{1}{2}\left(m^2_{h^0} - 2m_V^2\right)$ with $m_V = m_W(m_Z)$ for $V = W(Z)$ respectively. The forms of A_V and B_V are

$$A_V = \frac{\alpha\ p_1\cdot p_2}{4\pi m_V^2\delta_V}\frac{m_W}{g_2^3\sin^2\theta_W}\times\left[\frac{g_{h^0\tilde V\tilde V}g^2_{V\tilde V\tilde V'}}{m_{\tilde V}^2}N_{c,V}A_1(\tau_{\tilde V}) - \frac{2g_{h^0FF}g^2_{VFF'}}{m_F}N_{c,F}A_{1/2}(\tau_F) - \frac{g_{h^0SS}g^2_{VSS'}}{m_S^2}N_{c,S}A_0(\tau_S)\right],$$
$$B_V = -\frac{A_V}{p_1\cdot p_2}, \tag{B.8}$$

where the possible particles in the loops are $\tilde V, \tilde V' = F^+_\mu, F^3_\mu$, $F, F' = t_2, t_3, b_2, b_3, \tau_2, \tau_3, \nu_{\tau_2}, \nu_{\tau_3}$ and $S, S' = H^+, H^0$ respectively.

Since m_W and m_Z are much smaller than 750 GeV, one can further neglect the W and Z masses in Eq. (B.5) and Eq. (B.7). In this case, we have

$$\Gamma_{h^0\to\gamma\gamma} \simeq \frac{\alpha^2 m^3_{h^0}}{1024\pi^3}\left|\frac{A_1(\tau_V) + xA_0(\tau_S)}{v} + \frac{8\lambda_V A_{\frac{1}{2}}(\tau_{F_1})}{3(\lambda_V v - m_H)} + \frac{8\lambda_V A_{\frac{1}{2}}(\tau_{F_2})}{3(\lambda_V v + m_H)}\right|^2,$$
$$\Gamma_{h^0\to gg} \simeq \frac{\alpha_s^2 m^3_{h^0}}{512\pi^3}\left|\frac{2\lambda_V A_{\frac{1}{2}}(\tau_{F_1})}{\lambda_V v - m_H} + \frac{2\lambda_V A_{\frac{1}{2}}(\tau_{F_2})}{\lambda_V v + m_H}\right|^2,$$

$$\Gamma_{h^0\to Z\gamma} \simeq \frac{\alpha^2 m_{h^0}^3}{512\pi^3}\frac{1}{\sin^2\theta_W}\Big|\frac{\cos\theta_W}{v}A_1(\tau_V)+\frac{\cos\theta_W}{v}xA_0(\tau_S) + \frac{1-\frac{4}{3}\sin^2\theta_W}{\cos\theta_W}\left[\frac{2\lambda_V A_{\frac12}(\tau_{F_1})}{\lambda_V v-m_H}+\frac{2\lambda_V A_{\frac12}(\tau_{F_2})}{\lambda_V v+m_H}\right]\Big|^2,$$

$$\Gamma_{h^0\to ZZ} \simeq \frac{\alpha^2 m_{h^0}^3}{1024\pi^3}\frac{1}{\sin^4\theta_W}\Big|\frac{\cos^2\theta_W A_1(\tau_V)}{v}+\frac{x\cos^2\theta_W A_0(\tau_S)}{v} + \frac{\lambda_V}{\cos^2\theta_W}\sum_F N_{ZZ}^F\left[\frac{A_{\frac12}(\tau_{F_1})}{\lambda_V v-m_H}+\frac{A_{\frac12}(\tau_{F_2})}{\lambda_V v+m_H}\right]\Big|^2,$$

$$\Gamma_{h^0\to WW^*} \simeq \frac{\alpha^2 m_{h^0}^3}{512\pi^3}\frac{1}{\sin^4\theta_W}\Big|\frac{A_1(\tau_V)}{v}+\frac{xA_0(\tau_S)}{v}+\frac{2\lambda_V A_{\frac12}(\tau_{F_1})}{\lambda_V v-m_H}+\frac{2\lambda_V A_{\frac12}(\tau_{F_2})}{\lambda_V v+m_H}\Big|^2, \tag{B.9}$$

where we have defined

$$\tau_{F_1}=\frac{4(\lambda_V v-m_H)^2}{m_{h^0}^2},\ \tau_{F_2}=\frac{4(\lambda_V v+m_H)^2}{m_{h^0}^2},\ \tau_V=\frac{4m_{F_\mu}^2}{m_{h^0}^2},\ \tau_S=\frac{4m_{H^+}^2}{m_{h^0}^2},$$
$$\sum_F N_{ZZ}^F \equiv \left[3\Big(\frac12-\frac23\sin^2\theta_W\Big)^2+3\Big(-\frac12+\frac13\sin^2\theta_W\Big)^2+\Big(-\frac12+\sin^2\theta_W\Big)^2+\frac14\right],$$

θ_W is the weak mixing angle and x is introduced in Eq. (A.4) to parameterize the $h^0H^+H^-$ and $h^0H^0H^0$ couplings.

B.2. Partial widthes of the pseudo scalar A^0

Different from the h^0 case, only the vector-like fermions contribute to the decay $A^0\to VV'$. As a result, the expression of $\Gamma_{A^0\to VV^*}$ can be obtained from that of $\Gamma_{h^0\to VV^*}$ by following replacement:

$$m_{h^0}\to m_{A^0},\qquad A_{\frac12}(\tau_F)\to A_{\frac12}^A(\tau_F),\qquad A_1(\tau_V)\to 0,\qquad A_0(\tau_S)\to 0, \tag{B.10}$$

where the loop function $A_{\frac12}^A(\tau_F)$ is defined by

$$A_{\frac12}^A(x)=2xf(x)\ . \tag{B.11}$$

In the limit $x\to\infty$, $A_{\frac12}^A$ has following property

$$A_{\frac12}^A\to 2. \tag{B.12}$$

Appendix C. One loop RGE for Yukawa couplings

In this section, we present the one loop RGE running for all Yukawa couplings in Eq. (2.3) and gauge couplings g_3, $\tilde g_2$, $\tilde g_2$ and g_1, which correspond to the groups $SU(3)_c$, $SU(2)_1$, $SU(2)_2$ and $U(1)_Y$ respectively.

The RGEs of the Yukawa couplings are given by

$$4\pi^2\frac{dy_V^\Phi}{y_V^\Phi dt}=\frac{1}{2}\left[(y_T)^2+(y_B)^2\right]+\frac{7}{2}(y_V^\Phi)^2+\frac{1}{2}\left[3(y_{V'}^\Phi)^2+(y_{\tilde V}^\Phi)^2+(y_{\tilde V'}^\Phi)^2\right]-\left(8g_3^2+\frac{9}{4}\bar g_2^2+\frac{9}{4}\tilde g_2^2+\frac{1}{10}g_1^2\right),$$

$$4\pi^2\frac{dy_{V'}^\Phi}{y_{V'}^\Phi dt}=\frac{1}{2}\left[(y'_T)^2+(y'_B)^2\right]+\frac{7}{2}(y_{V'}^\Phi)^2+\frac{1}{2}\left[3(y_V^\Phi)^2+(y_{\tilde V}^\Phi)^2+(y_{\tilde V'}^\Phi)^2\right]-\left(8g_3^2+\frac{9}{4}\bar g_2^2+\frac{9}{4}\tilde g_2^2+\frac{1}{10}g_1^2\right),$$

$$4\pi^2\frac{dy_{\tilde V}^\Phi}{y_{\tilde V}^\Phi dt}=\frac{1}{2}\left[(y_N)^2+(y_E)^2\right]+\frac{5}{2}(y_{\tilde V}^\Phi)^2+\frac{1}{2}\left[3(y_V^\Phi)^2+3(y_{V'}^\Phi)^2+(y_{\tilde V'}^\Phi)^2\right]-\left(\frac{9}{4}\bar g_2^2+\frac{9}{4}\tilde g_2^2+\frac{9}{10}g_1^2\right),$$

$$4\pi^2\frac{dy_{\tilde V'}^\Phi}{y_{\tilde V'}^\Phi dt}=\frac{1}{2}\left[(y'_N)^2+(y'_E)^2\right]+\frac{5}{2}(y_{\tilde V'}^\Phi)^2+\frac{1}{2}\left[3(y_V^\Phi)^2+3(y_{V'}^\Phi)^2+(y_{\tilde V}^\Phi)^2\right]-\left(\frac{9}{4}\bar g_2^2+\frac{9}{4}\tilde g_2^2+\frac{9}{10}g_1^2\right),$$

$$4\pi^2\frac{dy_T}{y_T dt}=\frac{1}{2}\left[2(y_V^\Phi)^2+(y_T)^2+(y_B)^2\right]+\left[(y_T)^2+(y'_T)^2+(y_t)^2\right]-2(y_B)^2+\left(3(y_T)^2+3(y_B)^2+(y_N)^2+(y_E)^2\right)-\left(8g_3^2+\frac{9}{4}\bar g_2^2+\frac{17}{20}g_1^2\right),$$

$$4\pi^2\frac{dy_B}{y_B dt}=\frac{1}{2}\left[2(y_V^\Phi)^2+(y_T)^2+(y_B)^2\right]+\left[(y_B)^2+(y'_B)^2+(y_b)^2\right]-2(y_T)^2+\left(3(y_T)^2+3(y_B)^2+(y_N)^2+(y_E)^2\right)-\left(8g_3^2+\frac{9}{4}\bar g_2^2+\frac{1}{4}g_1^2\right),$$

$$4\pi^2\frac{dy_N}{y_N dt}=\frac{1}{2}\left[2(y_{\tilde V}^\Phi)^2+(y_N)^2+(y_E)^2\right]+\left[(y_N)^2+(y'_N)^2+(y_{\nu_\tau})^2\right]-2(y_E)^2+\left(3(y_T)^2+3(y_B)^2+(y_N)^2+(y_E)^2\right)-\left(\frac{9}{4}\bar g_2^2+\frac{9}{20}g_1^2\right),$$

$$4\pi^2\frac{dy_E}{y_E dt}=\frac{1}{2}\left[2(y_{\tilde V}^\Phi)^2+(y_N)^2+(y_E)^2\right]+\left[(y_E)^2+(y'_E)^2+(y_\tau)^2\right]-2(y_N)^2+\left(3(y_T)^2+3(y_B)^2+(y_N)^2+(y_E)^2\right)-\left(\frac{9}{4}\bar g_2^2+\frac{9}{4}g_1^2\right),$$

$$4\pi^2\frac{dy'_T}{y'_T dt}=\frac{1}{2}\left[2(y_{V'}^\Phi)^2+(y'_T)^2+(y'_B)^2\right]+\left[(y_T)^2+(y'_T)^2+(y_t)^2\right]-2(y'_B)^2+\left(3(y'_T)^2+3(y'_B)^2+(y'_N)^2+(y'_E)^2\right)-\left(8g_3^2+\frac{9}{4}\tilde g_2^2+\frac{17}{20}g_1^2\right),$$

$$4\pi^2\frac{dy'_B}{y'_B dt}=\frac{1}{2}\left[2(y_{V'}^\Phi)^2+(y'_T)^2+(y'_B)^2\right]+\left[(y_B)^2+(y'_B)^2+(y_b)^2\right]-2(y'_T)^2$$

$$
\begin{aligned}
&+\left(3(y'_T)^2+3(y'_B)^2+(y'_N)^2+(y'_E)^2\right)-\left(8g_3^2+\frac{9}{4}\tilde{g}_2^2+\frac{1}{4}g_1^2\right),\\
4\pi^2\frac{dy'_N}{y'_N dt}&=\frac{1}{2}\left[2(y^{\Phi}_{\tilde{V}'})^2+(y'_N)^2+(y'_E)^2\right]+\left[(y_N)^2+(y'_N)^2+(y_{\nu_\tau})^2\right]-2(y'_E)^2\\
&+\left(3(y'_T)^2+3(y'_B)^2+(y'_N)^2+(y'_E)^2\right)-\left(\frac{9}{4}\tilde{g}_2^2+\frac{9}{20}g_1^2\right),\\
4\pi^2\frac{dy'_E}{y'_E dt}&=\frac{1}{2}\left[2(y^{\Phi}_{\tilde{V}'})^2+(y'_N)^2+(y'_E)^2\right]+\left[(y_E)^2+(y'_E)^2+(y_\tau)^2\right]-2(y'_N)^2\\
&+\left(3(y'_T)^2+3(y'_B)^2+(y'_N)^2+(y'_E)^2\right)-\left(\frac{9}{4}\tilde{g}_2^2+\frac{9}{4}g_1^2\right),\\
4\pi^2\frac{dy_t}{y_t dt}&=\frac{1}{2}\left[(y_t)^2+(y_b)^2\right]+\left[(y_T)^2+(y'_T)^2+(y_t)^2\right]-2(y_b)^2,\\
&+\left(3(y'_T)^2+3(y'_B)^2+(y'_N)^2+(y'_E)^2\right)-\left(8g_3^2+\frac{9}{4}\tilde{g}_2^2+\frac{17}{20}g_1^2\right),\\
4\pi^2\frac{dy_b}{y_b dt}&=\frac{1}{2}\left[(y_t)^2+(y_b)^2\right]+\left[(y_B)^2+(y'_B)^2+(y_b)^2\right]-2(y_t)^2\\
&+\left(3(y'_T)^2+3(y'_B)^2+(y'_N)^2+(y'_E)^2\right)-\left(8g_3^2+\frac{9}{4}\tilde{g}_2^2+\frac{1}{4}g_1^2\right),
\end{aligned}
\tag{C.1}
$$

where y_V^{Φ} is the coupling coefficient for the $\bar{V}_L\Phi V_R$ interactions, and $y_{V'}^{\Phi}$, $y_{\tilde{V}}^{\Phi}$ and $y_{\tilde{V}'}^{\Phi}$ have similar definitions.

Above the vector-like fermion threshold, which is assumed to be $\lambda_V v$ in this work, the β functions of gauge couplings are given by

$$
\begin{aligned}
4\pi^2\frac{d}{dt}g_3&=-\frac{13}{3}g_3^3, & 4\pi^2\frac{d}{dt}\tilde{g}_2&=-\frac{3}{2}\tilde{g}_2^3\\
4\pi^2\frac{d}{dt}\tilde{g}_2&=-\frac{17}{6}\tilde{g}_2^3, & 4\pi^2\frac{d}{dt}g_1&=\frac{71}{15}g_1^3,
\end{aligned}
\tag{C.2}
$$

with the standard normalization $g_1^2=3g_Y^2/5$. Below the threshold, the β functions of the gauge couplings are given by

$$
4\pi^2\frac{d}{dt}g_3=-7g_3^3,\quad 4\pi^2\frac{d}{dt}g_2=-3g_2^3,\quad 4\pi^2\frac{d}{dt}g_1=7g_1^3,
\tag{C.3}
$$

with g_2 denoting the coupling of $SU(2)_L$.

References

[1] CMS note, CMS PAS EXO-15-004, Search for new physics in high mass diphoton events in proton-proton collisions at 13 TeV.

[2] ATLAS note, ATLAS-CONF-2015-081, Search for resonances decaying to photon pairs in 3.2 fb-1 of pp collisions, at vs = 13 TeV with the ATLAS detector.

[3] D. Buttazzo, A. Greljo, D. Marzocca, arXiv:1512.04929 [hep-ph].

[4] A. Falkowski, O. Slone, T. Volansky, arXiv:1512.05777 [hep-ph].

[5] K. Harigaya, Y. Nomura, arXiv:1512.04850 [hep-ph];
Y. Mambrini, G. Arcadi, A. Djouadi, arXiv:1512.04913 [hep-ph];
M. Backovic, A. Mariotti, D. Redigolo, arXiv:1512.04917 [hep-ph];
A. Angelescu, A. Djouadi, G. Moreau, arXiv:1512.04921 [hep-ph];

Y. Nakai, R. Sato, K. Tobioka, arXiv:1512.04924 [hep-ph];
S. Knapen, T. Melia, M. Papucci, K. Zurek, arXiv:1512.04928 [hep-ph];
A. Pilaftsis, arXiv:1512.04931 [hep-ph];
R. Franceschini, et al., arXiv:1512.04933 [hep-ph];
S. Di Chiara, L. Marzola, M. Raidal, arXiv:1512.04939 [hep-ph].
[6] T. Higaki, K.S. Jeong, N. Kitajima, F. Takahashi, arXiv:1512.05295 [hep-ph];
S.D. McDermott, P. Meade, H. Ramani, arXiv:1512.05326 [hep-ph];
J. Ellis, et al., arXiv:1512.05327 [hep-ph];
M. Low, A. Tesi, L.T. Wang, arXiv:1512.05328 [hep-ph];
B. Bellazzini, R. Franceschini, F. Sala, J. Serra, arXiv:1512.05330 [hep-ph];
R.S. Gupta, et al., arXiv:1512.05332 [hep-ph];
C. Petersson, R. Torre, arXiv:1512.05333 [hep-ph];
E. Molinaro, F. Sannino, N. Vignaroli, arXiv:1512.05334 [hep-ph].
[7] B. Dutta, et al., arXiv:1512.05439 [hep-ph];
Q.H. Cao, et al., arXiv:1512.05542 [hep-ph];
A. Kobakhidze, et al., arXiv:1512.05585 [hep-ph];
S. Matsuzaki, K. Yamawaki, arXiv:1512.05564 [hep-ph];
P. Cox, A.D. Medina, T.S. Ray, A. Spray, arXiv:1512.05618 [hep-ph];
D. Becirevic, E. Bertuzzo, O. Sumensari, R.Z. Funchal, arXiv:1512.05623 [hep-ph];
J.M. No, V. Sanz, J. Setford, arXiv:1512.05700 [hep-ph];
S.V. Demidov, D.S. Gorbunov, arXiv:1512.05723 [hep-ph];
W. Chao, R. Huo, J.H. Yu, arXiv:1512.05738 [hep-ph];
S. Fichet, G. von Gersdorff, C. Royon, arXiv:1512.05751 [hep-ph];
D. Curtin, C.B. Verhaaren, arXiv:1512.05753 [hep-ph];
L. Bian, N. Chen, D. Liu, J. Shu, arXiv:1512.05759 [hep-ph];
J. Chakrabortty, et al., arXiv:1512.05767 [hep-ph];
A. Ahmed, et al., arXiv:1512.05771 [hep-ph];
P. Agrawal, et al., arXiv:1512.05775 [hep-ph];
C. Csaki, J. Hubisz, J. Terning, arXiv:1512.05776 [hep-ph];
D. Aloni, et al., arXiv:1512.05778 [hep-ph];
Y. Bai, J. Berger, R. Lu, arXiv:1512.05779 [hep-ph].
[8] E. Gabrielli, et al., arXiv:1512.05961 [hep-ph];
R. Benbrik, C.H. Chen, T. Nomura, arXiv:1512.06028 [hep-ph];
J.S. Kim, J. Reuter, K. Rolbiecki, R.R. de Austri, arXiv:1512.06083 [hep-ph];
A. Alves, A.G. Dias, K. Sinha, arXiv:1512.06091 [hep-ph];
E. Megias, O. Pujolas, M. Quiros, arXiv:1512.06106 [hep-ph];
L.M. Carpenter, R. Colburn, J. Goodman, arXiv:1512.06107 [hep-ph];
J. Bernon, C. Smith, arXiv:1512.06113 [hep-ph].
[9] D. Barducci, A. Goudelis, S. Kulkarni, D. Sengupta, arXiv:1512.06842 [hep-ph];
M. Chala, M. Duerr, F. Kahlhoefer, K. Schmidt-Hoberg, arXiv:1512.06833 [hep-ph];
M. Bauer, M. Neubert, arXiv:1512.06828 [hep-ph];
J.M. Cline, Z. Liu, arXiv:1512.06827 [hep-ph];
W.S. Cho, D. Kim, K. Kong, S.H. Lim, K.T. Matchev, J.C. Park, M. Park, arXiv:1512.06824 [hep-ph];
L. Berthier, J.M. Cline, W. Shepherd, M. Trott, arXiv:1512.06799 [hep-ph];
J.S. Kim, K. Rolbiecki, R.R. de Austri, arXiv:1512.06797 [hep-ph];
X.J. Bi, Q.F. Xiang, P.F. Yin, Z.H. Yu, arXiv:1512.06787 [hep-ph];
M. Dhuria, G. Goswami, arXiv:1512.06782 [hep-ph];
J.J. Heckman, arXiv:1512.06773 [hep-ph];
W. Liao, H.q. Zheng, arXiv:1512.06741 [hep-ph];
F.P. Huang, C.S. Li, Z.L. Liu, Y. Wang, arXiv:1512.06732 [hep-ph];
F. Wang, L. Wu, J.M. Yang, M. Zhang, arXiv:1512.06715 [hep-ph];
T.F. Feng, X.Q. Li, H.B. Zhang, S.M. Zhao, arXiv:1512.06696 [hep-ph];
D. Bardhan, D. Bhatia, A. Chakraborty, U. Maitra, S. Raychaudhuri, T. Samui, arXiv:1512.06674 [hep-ph];
J. Chang, K. Cheung, C.T. Lu, arXiv:1512.06671 [hep-ph];
M.x. Luo, K. Wang, T. Xu, L. Zhang, G. Zhu, arXiv:1512.06670 [hep-ph];
X.F. Han, L. Wang, arXiv:1512.06587 [hep-ph];

H. Han, S. Wang, S. Zheng, arXiv:1512.06562 [hep-ph];
R. Ding, L. Huang, T. Li, B. Zhu, arXiv:1512.06560 [hep-ph];
I. Chakraborty, A. Kundu, arXiv:1512.06508 [hep-ph];
C. Han, H.M. Lee, M. Park, V. Sanz, arXiv:1512.06376 [hep-ph];
M.T. Arun, P. Saha, arXiv:1512.06335 [hep-ph];
W. Chao, arXiv:1512.06297 [hep-ph].

[10] P.S.B. Dev, D. Teresi, arXiv:1512.07243 [hep-ph];
A. Belyaev, G. Cacciapaglia, H. Cai, T. Flacke, A. Parolini, H. Serodio, arXiv:1512.07242 [hep-ph];
G.M. Pelaggi, A. Strumia, E. Vigiani, arXiv:1512.07225 [hep-ph];
U.K. Dey, S. Mohanty, G. Tomar, arXiv:1512.07212 [hep-ph];
C.W. Murphy, arXiv:1512.06976 [hep-ph];
S.F. Ge, H.J. He, J. Ren, Z.Z. Xianyu, Phys. Lett. B 757 (2016) 480, http://dx.doi.org/10.1016/j.physletb.2016.04.008, arXiv:1602.01801 [hep-ph].

[11] J. Gu, Z. Liu, arXiv:1512.07624 [hep-ph];
M. Cvetic, J. Halverson, P. Langacker, arXiv:1512.07622 [hep-ph];
W. Altmannshofer, J. Galloway, S. Gori, A.L. Kagan, A. Martin, J. Zupan, arXiv:1512.07616 [hep-ph];
Q.H. Cao, S.L. Chen, P.H. Gu, arXiv:1512.07541 [hep-ph];
S. Chakraborty, A. Chakraborty, S. Raychaudhuri, arXiv:1512.07527 [hep-ph];
M. Badziak, arXiv:1512.07497 [hep-ph];
K.M. Patel, P. Sharma, arXiv:1512.07468 [hep-ph];
S. Moretti, K. Yagyu, arXiv:1512.07462 [hep-ph];
W.C. Huang, Y.L.S. Tsai, T.C. Yuan, arXiv:1512.07268 [hep-ph].

[12] L.J. Hall, K. Harigaya, Y. Nomura, arXiv:1512.07904 [hep-ph];
J.A. Casas, J.R. Espinosa, J.M. Moreno, arXiv:1512.07895 [hep-ph];
J. Zhang, S. Zhou, arXiv:1512.07889 [hep-ph];
J. Liu, X.P. Wang, W. Xue, arXiv:1512.07885 [hep-ph];
K. Cheung, P. Ko, J.S. Lee, J. Park, P.Y. Tseng, arXiv:1512.07853 [hep-ph];
H. Davoudiasl, C. Zhang, arXiv:1512.07672 [hep-ph];
B.C. Allanach, P.S.B. Dev, S.A. Renner, K. Sakurai, arXiv:1512.07645 [hep-ph];
N. Craig, P. Draper, C. Kilic, S. Thomas, arXiv:1512.07733 [hep-ph];
Y. Hamada, T. Noumi, S. Sun, G. Shiu, arXiv:1512.08984 [hep-ph].

[13] J. Cao, C. Han, L. Shang, W. Su, J.M. Yang, Y. Zhang, Phys. Lett. B 755 (2016) 456, http://dx.doi.org/10.1016/j.physletb.2016.02.045, arXiv:1512.06728 [hep-ph].

[14] J. Zhang, S. Zhou, arXiv:1512.07889 [hep-ph];
M. Son, A. Urbano, arXiv:1512.08307 [hep-ph];
J. Cao, L. Shang, W. Su, Y. Zhang, J. Zhu, Eur. Phys. J. C 76 (5) (2016) 239, http://dx.doi.org/10.1140/epjc/s10052-016-4098-5, arXiv:1601.02570 [hep-ph].

[15] R. Martinez, F. Ochoa, C.F. Sierra, arXiv:1512.05617 [hep-ph];
S. Chang, Phys. Rev. D 93 (5) (2016) 055016, http://dx.doi.org/10.1103/PhysRevD.93.055016, arXiv:1512.06426 [hep-ph];
J. de Blas, J. Santiago, R. Vega-Morales, arXiv:1512.07229 [hep-ph];
S.M. Boucenna, S. Morisi, A. Vicente, arXiv:1512.06878 [hep-ph];
A.E.C. Hernandez, I. Nisandzic, arXiv:1512.07165 [hep-ph];
K. Das, S.K. Rai, arXiv:1512.07789 [hep-ph];
P.S.B. Dev, R.N. Mohapatra, Y. Zhang, J. High Energy Phys. 1602 (2016) 186, http://dx.doi.org/10.1007/JHEP02(2016)186, arXiv:1512.08507 [hep-ph].

[16] V. Miransky, M. Tanabashi, K. Yamawaki, Phys. Lett. B 221 (1989) 177;
V. Miransky, M. Tanabashi, K. Yamawaki, Mod. Phys. Lett. A 4 (1989) 1043;
W. Marciano, Phys. Rev. Lett. 62 (1989) 2793;
W.J. Marciano, Phys. Rev. D 41 (1990) 219;
W.A. Bardeen, C.T. Hill, M. Lindner, Phys. Rev. D 41 (1990) 1647.

[17] C.T. Hill, arXiv:hep-ph/9702320;
C.T. Hill, arXiv:hep-ph/9802216;
G. Cvetic, Rev. Mod. Phys. 71 (1999) 513.

[18] B.A. Dobrescu, C.T. Hill, Phys. Rev. Lett. 81 (1998) 2634;
R.S. Chivukula, B.A. Dobrescu, H. Georgi, C.T. Hill, Phys. Rev. D 59 (1999) 075003;

B.A. Dobrescu, Phys. Rev. D 63 (2001) 015004.
[19] H.-J. He, C.T. Hill, T.M.P. Tait, Phys. Rev. D 65 (2002) 055006.
[20] E. Malkawi, T.M.P. Tait, C.P. Yuan, Phys. Lett. B 385 (1996) 304, http://dx.doi.org/10.1016/0370-2693(96)00859-3, arXiv:hep-ph/9603349.
[21] E. Malkawi, T. Tait, C.-P. Yuan, Phys. Lett. B 385 (1996) 304;
D. Muller, S. Nandi, Phys. Lett. B 383 (1996) 345.
[22] H.-J. He, T.M.P. Tait, C.-P. Yuan, Phys. Rev. D 62 (2000) 011702;
X.F. Wang, C. Du, H.J. He, Phys. Lett. B 723 (2013) 314, http://dx.doi.org/10.1016/j.physletb.2013.05.015, arXiv:1304.2257 [hep-ph].
[23] N.G. Deshpande, J.F. Gunion, B. Kayser, F.I. Olness, Phys. Rev. D 44 (1991) 837, http://dx.doi.org/10.1103/PhysRevD.44.837.
[24] G. Aad, et al., ATLAS Collaboration, Phys. Lett. B 710 (2012) 49.
[25] S. Chatrachyan, et al., CMS Collaboration, Phys. Lett. B 710 (2012) 26.
[26] V. Khachatryan, et al., CMS Collaboration, Phys. Rev. D 93 (1) (2016) 012001, http://dx.doi.org/10.1103/PhysRevD.93.012001, arXiv:1506.03062 [hep-ex].
[27] ATLAS Collaboration, Phys. Rev. D 91 (11) (2015) 112011, arXiv:1503.05425 [hep-ex];
ATLAS Collaboration, J. High Energy Phys. 1508 (2015) 105, arXiv:1505.04306 [hep-ex];
CMS Collaboration [CMS Collaboration], CMS-PAS-B2G-15-006.
[28] Roberto Franceschini, et al., arXiv:1512.04933 [hep-ph].
[29] https://twiki.cern.ch/twiki/bin/view/LHCPhysics/CERNYellowReportPageAt1314TeV.
[30] G.C. Branco, P.M. Ferreira, L. Lavoura, M.N. Rebelo, M. Sher, J.P. Silva, Phys. Rep. 516 (2012) 1, http://dx.doi.org/10.1016/j.physrep.2012.02.002, arXiv:1106.0034 [hep-ph].
[31] Ryosuke Sato, Kohsaku Tobioka, arXiv:1605.05366.
[32] ATLAS note, ATLAS-CONF-2016-059, Search for scalar diphoton resonances with 15.4 fb^1 of data collected at $\sqrt{s} = 13$ TeV in 2015 and 2016 with the ATLAS detector.
[33] CMS note, CMS PAS EXO-16-027, CMS Physics Analysis Summary.
[34] Marcela Carena, Ian Low, Carlos E.M. Wagner, J. High Energy Phys. 08 (2012) 060.